JOURNAL OF GEOPHYSICAL RESEARCH: OCEANS, VOL. 118, 6807–6823, doi:10.1002/2013JC008963, 2013

Coastal cliff-top ground motions as proxies for environmental processes

Emma C. Norman,[1] Nick J. Rosser,[1] Matthew J. Brain,[1] David N. Petley,[1] and Michael Lim[2]

Received 21 March 2013; revised 29 October 2013; accepted 12 November 2013; published 12 December 2013.

[1] A two-year dataset of coastal cliff microseismic ground motions is used to explore energy transfer to a cliff. The long-term dataset enables us to characterise cliff motion responses to a wide range of environmental processes and examine whether short-term characteristics are representative of the long-term. We examine whether cliff-top motions are reliable proxies for environmental processes to inform future investigations into the drivers of erosion. The study is based at an actively eroding, macrotidal, hard rock cliffed coast where considerable intra-annual variability in wave, tide, and storm conditions permit the examination of a full range of environmental permutations. Three frequency bands of ground motion are identified that represent wind and wave processes that transfer energy to the cliff. Examining mean energy transfer by aggregating the frequency bands by sea water elevation reveals a notable departure from tidal inundation duration alone, of relevance to understanding the timing, duration and intensity of effective processes of erosion. Peak energy transfer to the cliff face occurs during the largest storms where water levels significantly exceed those of tidal inundation rather than at locations most frequently inundated by tides. We anticipate it is therefore these conditions that are likely to be most effective in eroding hard rock coasts, rather than periods which accrue energy transfer associated with still or calm waters, and hence tidally modulated inundation may not relate well to coastal erosion. Promisingly, despite signal overlap and noise, cliff-top motions can be used as proxies for the processes that transfer energy to the coast.

Citation: Norman, E. C., N. J. Rosser, M. J. Brain, D. N. Petley, and M. Lim (2013), Coastal cliff-top ground motions as proxies for environmental processes, *J. Geophys. Res. Oceans*, *118*, 6807–6823, doi:10.1002/2013JC008963.

1. Introduction

[2] High-resolution studies of hard rock coastal cliff erosion using terrestrial laser scanning (TLS) have found poor correlations between rockfall activity and regional-scale environmental monitoring datasets, resulting in uncertainty over the role of environmental controls in short and long-term hard rock cliff erosion, and therefore also of the underlying failure mechanisms [*Rosser et al*., 2007; *Lim et al*., 2010]. Studies of cliffs in softer materials have successfully attributed erosion to marine and weather conditions [*Sallenger et al*., 2002; *Collins and Sitar*, 2008; *Young et al*., 2009; *Quinn et al*., 2010] due to more rapid cliff responses to environmental forcing, yet equivalent studies on hard rock cliffs are few. Progress has been made with short-term ($<10^1$ yr) high-resolution monitoring [*Dewez et al*., 2009; *Barlow et al*., 2012], giving insight into annual and inter-annual variability in erosion in response to seasonal or extreme [*Hapke and Green*, 2006] conditions. A key issue is measuring, monitoring and characterising those conditions which influence the erosion of the coast, locally to the cliff and in a manner that is relevant to driving erosion.

[3] Wave energy delivery to the cliff toe is widely recognized as a key driver of coastal cliff erosion, powering abrasion and impact loads [e.g., *Trenhaile*, 1987; *Bray and Hooke*, 1997; *Anderson et al*., 1999; *Walkden and Hall*, 2005]. Models of tidal inundation, which equate inundation duration to exposure to wave attack, have widely been used to consider the vertical distribution of wave energy delivery and erosion of the cliff face [*Trenhaile and Layzell*, 1981; *Carr and Graff*, 1982; *Trenhaile*, 2000]. Whilst studies that have compared tidal data with observed rockfall data have found some statistically significant relationships between tide heights and rockfall volumes [*Rosser et al*., 2007; *Lim et al*., 2010], the relationships have been weak. This suggests that either other factors are involved, such as wave climate, or that tides monitored at some distance and then modelled more locally to the cliff may not be representative of the processes in action. As yet, the distribution of energy delivery to the cliff resulting from tidal inundation duration has not been quantified.

Additional supporting information may be found in the online version of this article.

[1]Department of Geography, University of Durham, Science Laboratories, South Road, Durham, UK.
[2]Department of Geography & Environment, Northumbria University, Newcastle upon Tyne, UK.

Corresponding author: E. C. Norman, Department of Geography, University of Durham, Science Laboratories, South Rd., Durham, DH1 3LE, UK. (e.c.norman@durham.ac.uk)

2169-9275/13/10.1002/2013JC008963

[4] Monitoring the conditions a cliff is exposed to is complex because of the range of both marine and subaerial processes operating at and near cliffs, and because they are highly variable spatially (up cliff face, across the foreshore and beyond) and temporally. The spatial variability of marine conditions, which are closely controlled by seabed and foreshore topography, the direction of incoming energy (i.e., wind and wave directions) and the interactions between variables, means monitoring discrete marine variables in isolation may not provide sufficient representation of the conditions experienced by the cliff.

[5] Microseismic ground motion has long been known to be generated by ocean waves in both shallow water as primary microseisms that have the same periodicity as the incoming ocean waves [*Hasselmann*, 1963; *Haubrich et al*., 1963; *Hedlin and Orcutt*, 1989], and in deeper water via double frequency (DF) microseisms generated by the constructive superposition of waves of the same period travelling in opposite directions [*Longuet-Higgins*, 1950]. Recent studies using cliff seismometers have identified that the microseismic motion of cliffs is influenced by tides, nearshore gravity and infragravity waves, with seismic sources local to the cliff across the intertidal zone, within the nearshore coastal zone and offshore [*Adams et al*., 2002, 2005; *Lim et al*., 2011; *Young et al*., 2011, 2012; *Dickson and Pentney*, 2012]. Different frequency bands of cliff motion have been observed to represent a variety of wave processes: High frequency cliff shaking has been attributed to wave impacts and observed at frequencies of ~20 Hz [*Adams et al*., 2005], > 0.2 Hz [*Young et al*., 2011, 2012] and >7 Hz [*Dickson and Pentney*, 2012]; Single frequency microseisms have been observed at cliff top seismometers over frequency ranges of 0.1–0.05 Hz [*Adams et al*., 2005; *Young et al*., 2011], 0.1–0.04 Hz [*Young et al*., 2012] and double frequency microseisms at frequencies 0.1–0.2 Hz [*Young et al*., 2012], 0.1–0.3 Hz [*Young et al*., 2011]; In addition *Young et al*. [2011, 2012] also identified signals < 0.04 Hz potentially representing nearshore infragravity waves and tilt caused by loading of the foreshore.

[6] Monitoring microseismic cliff motions has shown that foreshore geometry holds a strong control on energy dissipation across the foreshore [*Dickson and Pentney*, 2012; *Young et al*., 2012] and that ground motion rapidly attenuates inland and so can only have a localised effect on rock mass strength, if any [*Adams et al*., 2005; *Young et al*., 2012]. Cliff motions potentially may be used to explore and quantify a range of environmental forces acting on coastal cliffs [*Adams et al*., 2002, 2005; *Lim et al*., 2011; *Young et al*., 2011, 2012; *Dickson and Pentney*, 2012]. To date, cliff-top motions have only been examined for short periods of time e.g., < 5 months [e.g., *Adams et al*., 2002, 2005; *Lim et al*., 2011; *Young et al*., 2011, 2012; *Dickson and Pentney*, 2012]. As yet it has not been attempted to link cliff motions with observed erosion, and as proxies of environmental processes acting on a cliff, cliff motions may provide a useful tool to explore the environmental controls of erosion. Before links between cliff motions and erosion can be considered we need to explore the characteristics of cliff motions over longer timescales and examine whether the short-term characteristics observed are representative of the long-term.

[7] We present a two-year cliff-top ground motion dataset to explore and define the characteristic ground motion signals and to attribute and quantify sources of energy delivery to a rocky coast. We consider how these ground motions vary in response to the prevailing environmental conditions concurrently monitored. We examine whether cliff-top motions are reliable proxies for environmental processes, and consider the insight gained from comparison of the various sources of ground motion. A consideration of the direct efficacy of ground motions as drivers of erosion, via for example the cyclic accumulation of damage [e.g., *Adams et al*., 2005] is beyond the scope of this paper, but we consider this elsewhere [*Brain et al.*, 2013]; instead here we aim to characterise the nature of the ground motion frequency response and relate this to prevailing environmental conditions to inform future investigations into the drivers of erosion.

2. Study Site

[8] The cliffs of the North York Moors National Park (Figure 1) are comprised of near-vertical rock faces cut into interbedded Lower Jurassic shales, mudstones and limestones, capped with fine grained sandstone and glacial till [*Rawson and Wright*, 1992]. At our site the rock cliff face reaches 65 m above the cliff toe. The cliffs are fronted by an extensive low angle ($< 2^o$) essentially sediment-free foreshore platform that at low-tides extends to > 200 m offshore (Figure 1). Analysis of historic maps derives an average annual retreat rate of 0.05 m yr^{-1} since 1895 [*Agar*, 1960; *Lim et al*., 2009], yet more recent high-resolution monitoring suggest lower mean erosion rates [*Rosser et al*., 2013].

[9] The coast experiences semi-diurnal tides that cycle between spring and neap highs over a *c*. 6 m range (Figure 1), inundating > 3 m of the cliff toe during high spring tides, the vertical reach of which is extended during storms and high swells and by run-up from waves approaching from the open aspect coast of the North Sea. The cliff toe elevation is 1.6 m ordnance datum (OD), mean high water neap (MHWN) tide level occurs at 1.4 m OD which means that only during spring high tides does the sea interact directly with the cliff face. The coastline is oriented east-west and so remains sheltered from prevailing south-westerly winds. During the 2 year monitoring period the maximum wave height recorded at the wave buoy was 6.5 m, and the significant wave height was 2.23 m. The fetch at this site for most directions is limited by the boundary coasts of the North Sea, with a maximum fetch of approximately 860 km. Between approximately N - NNE the fetch extends much further into the Norwegian Sea, with its maximal extent being seasonally limited by sea ice cover.

3. Methods

3.1. Field Data

[10] A single Guralp 6TD seismometer (S1) was installed at the cliff top within glacial till, *c*. 70 m OD (Figure 1), approximately 20 m inland from the cliff edge. 100 Hz data was captured for a 2 year period covering two winter periods (July 2008–July 2010). 186 days of data were not used during this period due to loss of power, instrument

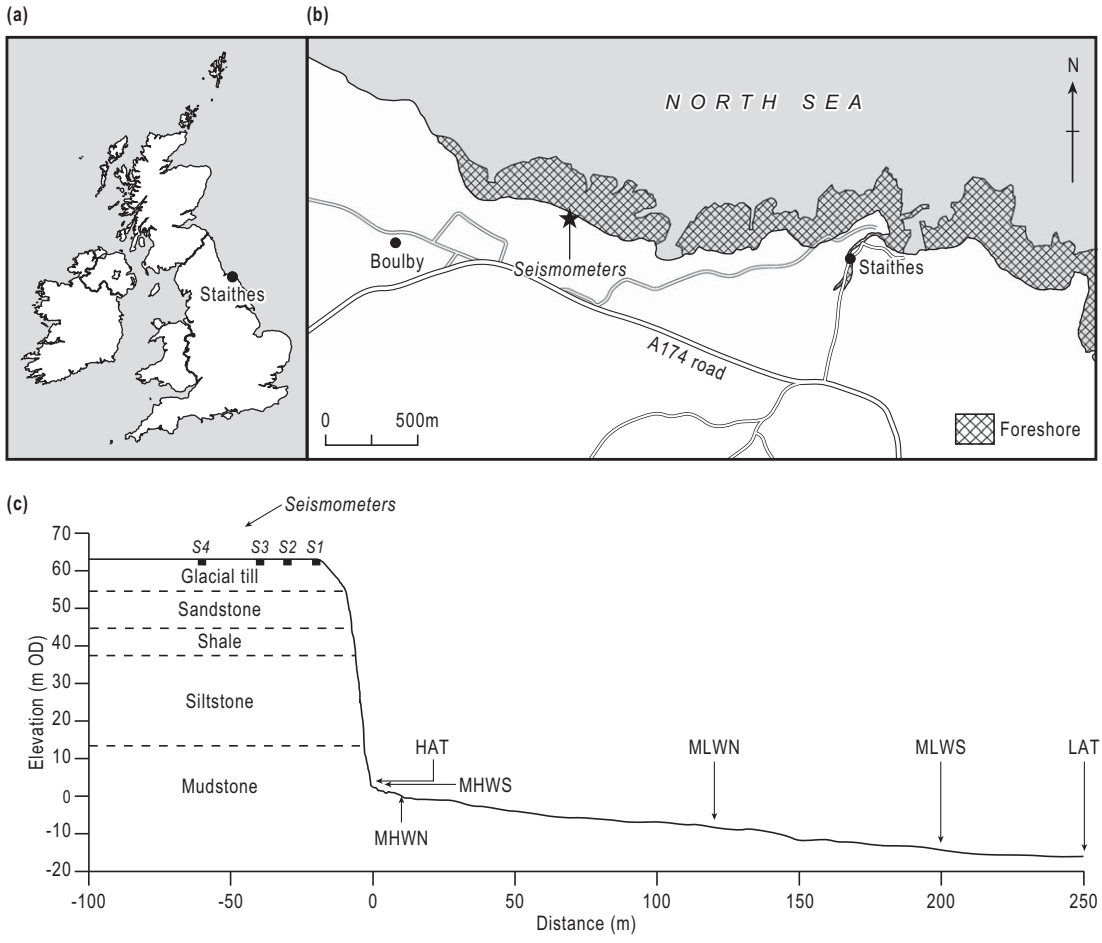

Figure 1. (a) Study site location on the North Yorkshire coast, UK; (b) Seismometers location at Boulby, near Staithes; (c) Cliff and intertidal foreshore profile and seismometer locations. Horizontal distance is defined from the cliff toe. Cliff toe elevation is 1.6 m OD. Tidal mean and extreme elevations: HAT = highest astronomical tide; MHWS = mean high water spring; MHWN = mean high water neap; MLWN = mean low water neap; MLWS = mean low water spring; LAT = lowest astronomical tide. Seismometers are at the following distances from the cliff edge: S1 = 20 m, S2 = 30 m, S3 = 40 m and S4 = 60 m.

failure and removal of days when we were in the field. The instrument has a flat frequency response of 0.033–100 Hz (period response range of 30–0.01 s). We recorded velocity data (ms^{-1}) in three axes (vertical, z; north-south, n; and east-west, e). We report here only z component data and focus our analysis on the frequency range 0.14–50 Hz (the Nyquist frequency) to overcome the potential data contamination effects of tilt [see *Young et al*., 2012]. In addition the 6TD instrument noise was significant > 10 s. Data from an array of a further three identical instruments (S2–S4), positioned in a coast-normal transect at + 10, + 20, and + 40 m intervals inland from S1 (Figure 1), are reported below to consider signal attenuation effects. Concurrent environmental data were collated at 60 min intervals from the closest source possible: wind speed and direction data from the Loftus Met Office station *c*. 3 km north west; UK National Tide Gauge Network data from Whitby *c*. 20 km south east; and, Cefas WaveNet wave buoy data offshore of the Tees estuary *c*. 20 km north west. Cliff and foreshore geometry (Figure 1) were captured using ground-based and airborne laser scanning, reported elsewhere [*Rosser et al*., 2005]. At site sea-state and nearshore conditions (wave, set-up and water heights) were modelled from wave buoy data using a wave transformation model based upon *Battjes and Stive* [1985] (see supporting information) to increase the representativeness of the data to local site conditions.

3.2. Seismic Data Analysis and Assumptions

[11] Seismic data were processed using PQLX to derive hourly average power spectral density (PSD), at the resolution of the environmental data [*Norman*, 2012]. *McNamara and Buland* [2004] provide a detailed explanation of the steps taken to calculate the PSD. In summary PQLX calculates the average PSD for overlapping hours of data using a fast Fourier transform with the output as decibels (dB) (calculated as $10\log_{10}((m/s)^2/Hz)$). Power describes the rate at which energy is transferred to the cliff. From power, energy delivery (μJ) was calculated (see supporting information).

[12] We make the following assumptions in analysing this data. First, microseismic ground motion measured at a point which originates from distributed sources is subject to complex and varied signal paths and attenuation. Recorded ground motion reflects both source characteristics but also the effects of the travel path. Second, although highly effective processes of erosion may be microseismically quiet at this scale of investigation (e.g., weathering, abrasion, freeze-thaw), the conditions that catalyse such processes, for example wave climate, are not.

4. Results and Interpretation

4.1. Coastal Cliff Ground Motion Characteristics

4.1.1. Observed Frequency Bands of Cliff-Top Ground Motions

[13] By comparing power spectrograms of the vertical motions over the period range 0.02–10 s (50–0.1 Hz) with the time series of local marine and weather data, three frequency bands of cliff motions have been identified which appear to be generated by prevailing environmental conditions. We consider 2 years of data to examine these ground motions and the environmental processes that generate them. It is clear that the site has a complex seismic response, with no point in time having a perfectly quiet seismic signature. Whilst we define discrete responses in specific frequency bands below, there is some overlap between bands, and so the processes we consider may superimpose across these bands. But the characteristics defined are those which appear to dominate the signal power in these particular frequency bands and the overall seismic response of this site. Figure 2 outlines the three frequency bands that exhibit discrete characteristics and the typical environmental conditions that occur when each is observed, described as:

4.1.1.1. Microseism Frequency Band (MS)

[14] Increased powers in the period band 1–10 s (1–0.01 Hz) often occur when increased wave heights ($>$ 2 m) are recorded at the wave buoy (Figure 2). Microseisms are typically observed within the period range 1–30 s, although the range detected at sites varies dependent on local physiographic conditions and their control on ocean wave characteristics and seismic wave transmission [e.g., *Hedlin and Orcutt*, 1989; *Cessaro*, 1994; *Webb*, 1998; *Bromirski and Duennebier*, 2002]. The MS frequency band power corresponds to increased power at the high frequency bands (non-anthropogenic) which appear to be associated with incoming waves and increased winds (Figure 2), suggesting locally generated ground motions. On occasion MS power does not correspond with these signals or the wave buoy data, indicating MS signals generated at more distal locations from the site.

4.1.1.2. High Tide Frequency Band (HT)

[15] Twelve hour spaced high power signals are commonly observed in the high frequency range 0.02–0.9 s (1.1–50 Hz) (Figure 2). These are coincident with some but not every high tide, and at times last longer than the duration of the high tide alone. The HT signal is more prominent during periods of increased MS power, and higher wave heights recorded at the buoy, suggesting the influence of ocean waves on this frequency band. These characteristics suggest the HT frequency band represents shaking of the cliff mass in response to large waves during high tides of sufficient height for water levels to reach and exceed the cliff toe. Below we consider whether it is possible to discern the actual mechanism that drives this ground motion from this data. Similar signals have been observed by *Adams et al*. [2005] and *Young et al*. [2011, 2012], albeit over varying frequency ranges, and it is anticipated that the HT frequency band observed here represents the same phenomenon with the specific frequency response modified by conditions at this site.

4.1.1.3. Wind Frequency Band (WI)

[16] Sporadic increases in power similar to values observed in HT are observed within the 0.02–0.08 s (12.5–50 Hz) frequency band. WI signal power increases and decreases in tandem with wind velocity, a correlation observed particularly when winds exceed 3 ms^{-1} (Figure 2). The intermittent, high power, high frequency and stochastic nature of this response suggests the influence of wind locally acting upon the cliff face. These signal characteristics match the observations of wind seismic noise studies where wind velocities of 3 ms^{-1} and stronger result in a significant non-linear increase of seismic energy to the ground surfaces at frequencies of 15–60 Hz (0.066–0.017 s) [*Young et al*., 1996] or lower frequencies [e.g., *Bungum et al*., 1985; *Given*, 1990; *Gurrola et al*., 1990] as low as 1 Hz [*Withers et al*., 1996].

[17] Within some of the analysis individual periods of cliff ground motion have been selected to represent different frequency bands. 0.022 s has been selected to represent wind (WI), and 0.104 s selected to represent high tide wave impacts (HT) as these periods best represent the characteristics of the bands, and also 0.022 s is least affected by the overlap with HT. Three microseism (MS) periods (1 s, 2 s, and 5 s) have been selected to examine variations in microseism characteristics within the MS band. Exploring a number of MS periods may help identify the different processes generating this band of cliff motions. 2 s was the shortest wave period, and 5 s was the mean wave period, recorded by the buoy. 5 s is also the wave period typically associated with double frequency microseisms in global seismic noise models [e.g., *Peterson*, 1993]. 5 s double frequency microseisms are generated by swell waves of 10 s, and at the buoy 10 s waves made up only 8% of the monitored hourly maximum wave periods recorded. 1 s period has been selected as it may represent a number of nearshore processes: 1 s waves are shorter than the wave periods recorded at the buoy, therefore may represent double frequency microseisms, generated by the superposition of 2 s ocean waves. Alternatively seismic signals of 1 s period may represent short period waves generated near the cliff. The shorter period MS signals may also partially represent overlap with the HT band. Exploring these MS periods will help distinguish the active processes and may help identify whether the MS periods represent single or double frequency microseisms, and therefore their source locations.

[18] In addition to the marine and wind signals other high frequency signals are apparent in the spectrogram (Figure 2):

4.1.1.4. Anthropogenic Frequency Bands (AN)

[19] Within the high-frequency range 0.05–0.9 s (1.1–20 Hz) two intermittent, short-period signals are tightly constrained within the frequency bands 0.5–0.9 s (1.1–2 Hz)

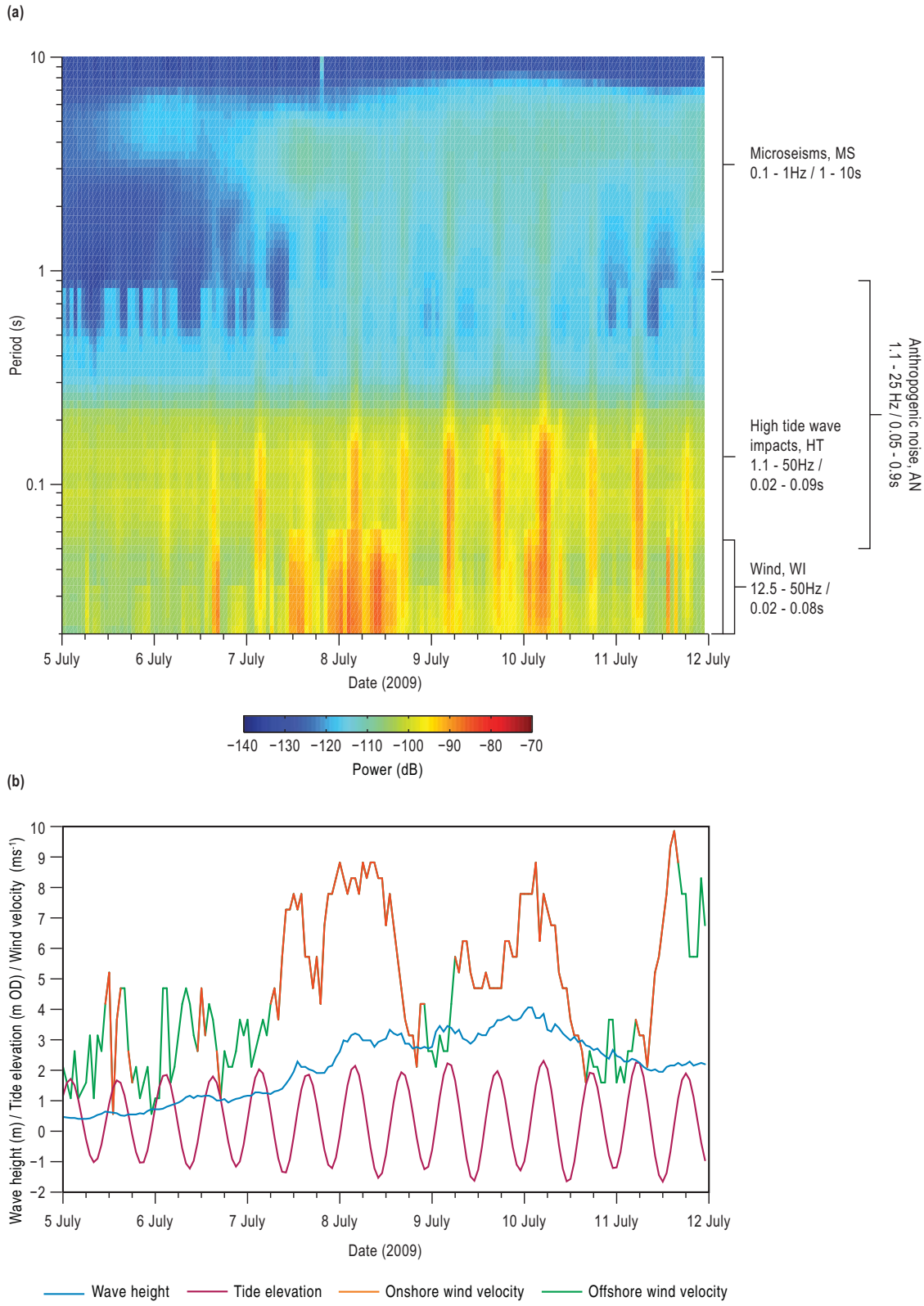

Figure 2. Cliff-top ground motion response to tides, waves and wind over 1-week. (a) Power spectrogram (z component, vertical motions). Three frequency bands are identified across the 0.1–50 Hz/0.02–10 s spectrum of ground motions, each representing different wind and wave processes: Wind (WI); High tide wave impacts (HT); Microseisms (MS). In addition a band of anthropogenic noise is identified (AN). (b) Tide elevation, wave heights and wind velocity.

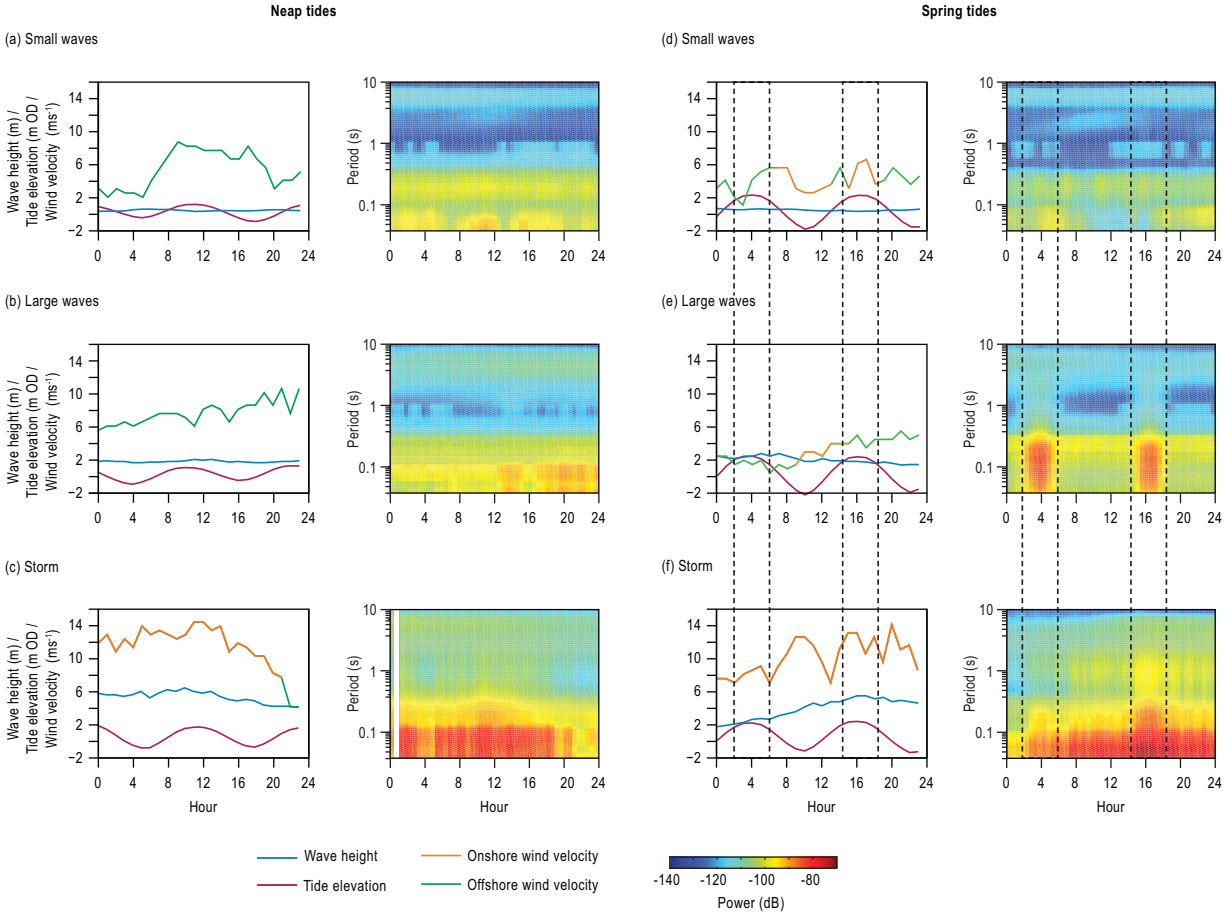

Figure 3. Cliff-top ground motion response to (a) neap tides combined with small waves ~0.5 m (10th percentile of wave heights during the monitoring period) (04/08/10); (b) neap tides combined with large waves ~2 m (90th percentile of wave heights during the monitoring period) (11/07/08); (c) neap tides combined with a storm (11/22/08); and (d) spring tides combined with small waves ~0.5 m (05/15/10); (e) spring tides combined with large waves ~2 m (10/05/09); f) spring tides combined with a storm (12/17/09). Power spectrograms are from the z component (vertical motions). N.B. Dashed lines in d – f delineate when the cliff face was inundated. The white band in spectrogram (c) denotes missing data.

and 0.05–0.5 s (2–20 Hz) (Figure 2). The sharply defined frequency bands and the binary nature of the associated signal power suggests that these motions are most likely generated by anthropogenic activity. The most likely source is the 24 h Boulby Mine whose tailings facility containing pumps is approximately 150 m from the monitoring site. These anthropogenic signals are discounted from further analysis here.

4.1.2. Temporal Variations of the Ground Motion Signals

[20] We examine the characteristics of HT, MS and WI in varying tides, waves and winds to identify the specific conditions required to generate these ground motions at the study site. First we examine typical 1 day examples of neap and spring tides during both quiet wave conditions (waves < 0.5 m), during large waves (> 2 m), and during storms (Figure 3) to explore the full range of conditions experienced by the cliff. We also consider a neap to spring tide cycle over a 2 week period (Figure 4), and the full 2 year dataset covering 2 winter periods (Figures 5 and 6).

[21] Figure 3 shows that HT excitation of the cliff is not conditional upon high tides alone. Increases in signal power occur only during spring tides when accompanied by waves > 2 m (Figure 3e). As water levels reach the cliff toe during high spring tides, power increases and then falls as the tide recedes (Figure 3e). During spring high tides the mean water level rises above the cliff toe to approximately 3.3 m OD, providing sufficient water depths to enable incoming waves to impact and then run-up the cliff face. The absence of a high tide HT signal in the spring tide small wave scenario (Figure 3d) suggests that combined tide and wave height is required to enable energy transfer to the cliff observed here. No HT signal is observed during the neap tides with either small (Figure 3a) or large waves (Figure 3b) as mean high water neap (MHWN) tide peaks below the break in slope at the cliff toe (*c*. 1.4 m OD), and

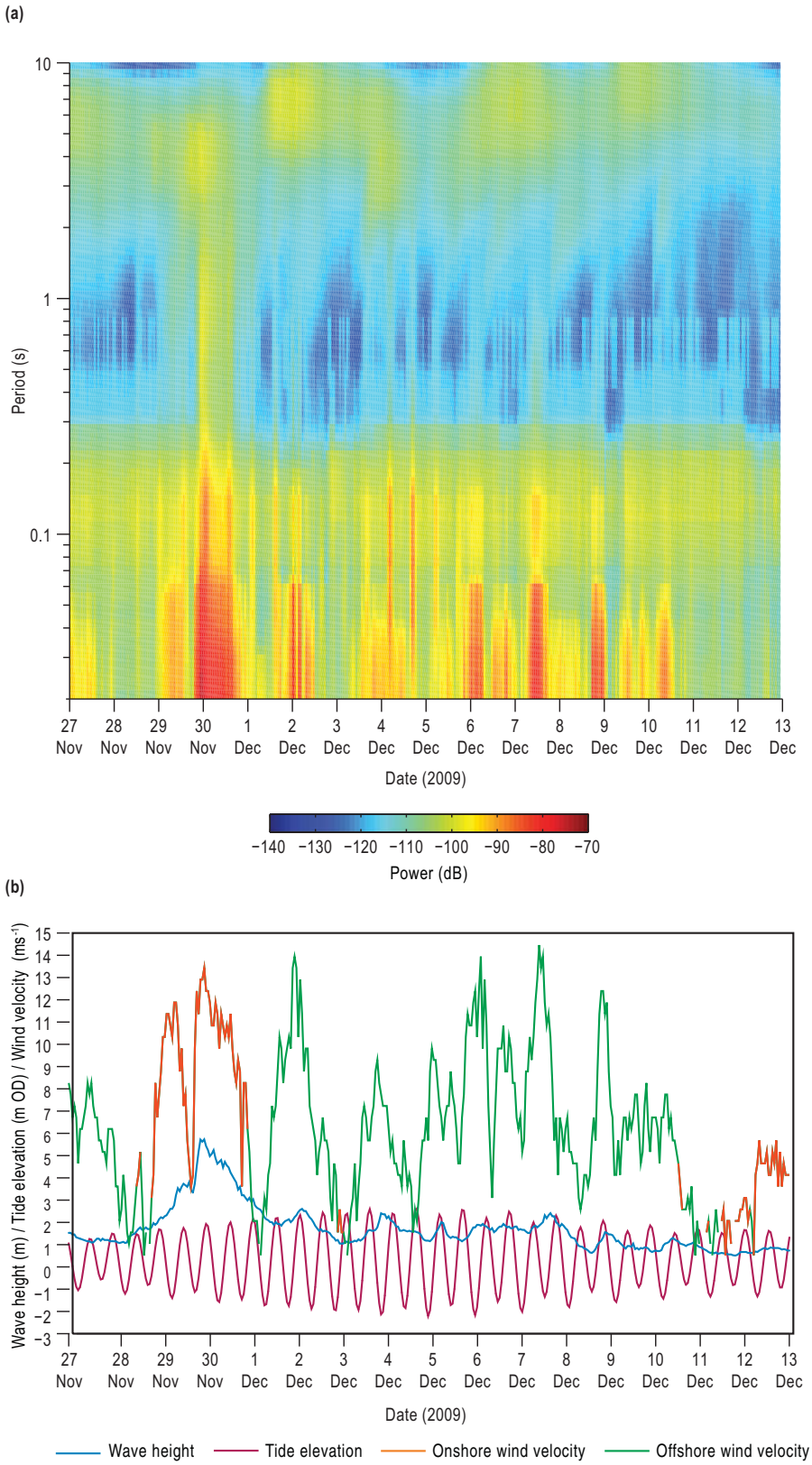

Figure 4. Cliff-top ground motion response to tides, waves and wind over a 2 week neap-spring-neap tidal cycle. (a) Power spectrogram (z component, vertical motions) for the 0.1–50 Hz/0.02–10 s spectrum of ground motions. (b) Tide elevation, wave heights and wind velocity.

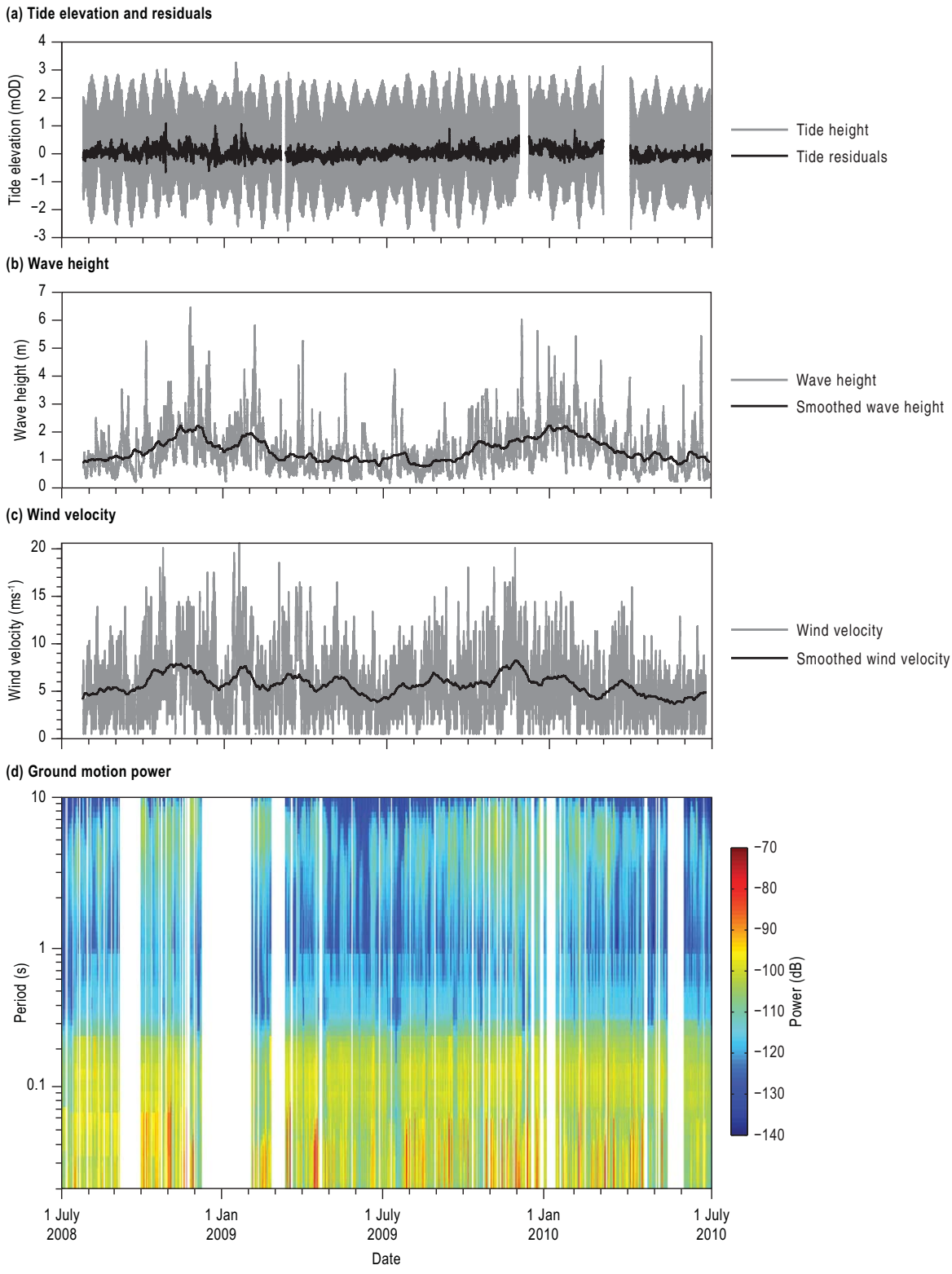

Figure 5. Environmental conditions and ground motion power over the 2 year monitoring period (July 2008–July 2010). (a) Tide elevations and residuals modelled for Boulby from Whitby tide gauge data; (b) Wave heights measured at offshore wave buoy, raw and smoothed using a moving average over 30 day periods; (c) Wind velocity measured near Boulby, raw and smoothed using a moving average over 30 day periods; (d) Power spectrogram (z component, vertical motions) for the 0.1–50 Hz/0.02–10 s spectrum of ground motions. The white bands in the spectrogram denote missing data.

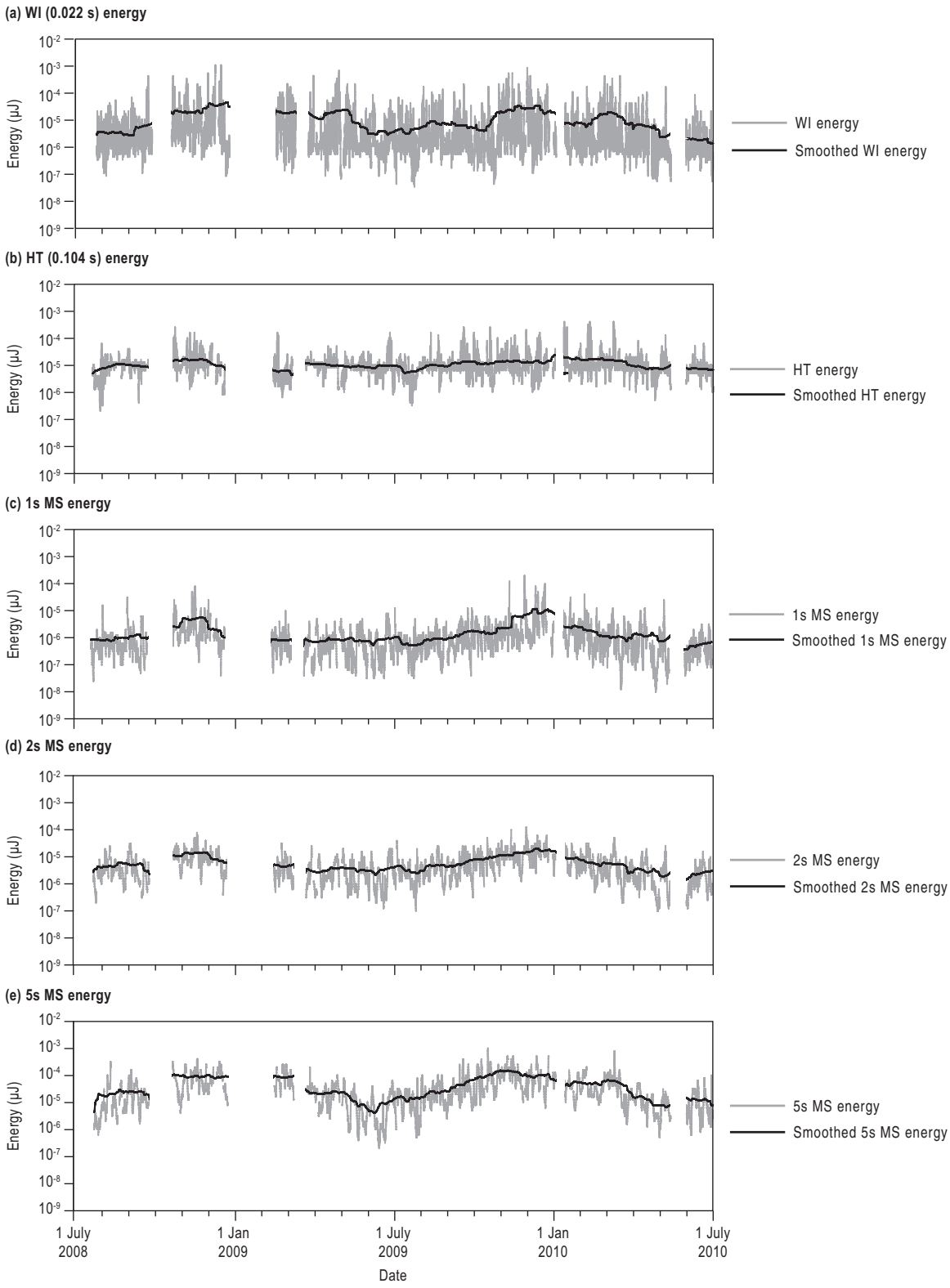

Figure 6. Ground motion energy (raw and smoothed) of periods selected to represent each of the three frequency bands, WI, HT and MS, over the 2 year monitoring period (July 2008–July 2010). Smoothed energy was smoothed using a moving average over 30 day periods. (a) WI (0.022 s); (b) HT (0.104 s); (c) 1 s MS; (d) 2 s MS; (e) 5 s MS. The WI and HT periods have been selected as they best represent the characteristics of each band. The three MS periods have been selected to examine variations in microseism characteristics within the MS band.

therefore only limited wave energy is transferred directly to the cliff.

[22] During the times where waves at the wave buoy are small (Figure 3a and 3d) higher signal power within the MS band is observed between 4–8 s. Because of the quiet local wave conditions monitored at the buoy this signal likely represents more distal waves generating double frequency microseisms. Large waves recorded at the wave buoy during both neap and spring tides (Figure 3b and e) increase signal power within the MS band across a larger period range (1–10 s), irrespective of mean water elevation, also suggesting MS generation seawards of the intertidal zone by varying wave periods. This period range at the study site may represent microseism generation by both single and double frequency mechanisms.

[23] During times with large waves and high spring tides (Figure 3e), the MS band periods (1–3 s) are strongly modulated by the tide indicating either these shorter period signals may be being generated across the intertidal foreshore platform, or that the HT shaking extends into these periods. The power of these signals increases with increasing water depth and the shoreward transgression of the water front, enabling greater levels of seismic energy to be transferred.

[24] Across the tidal scenarios considered, WI is generated when wind velocities exceed 3 ms^{-1}. Whilst signal power decreases (Figure 3c) and increases (Figure 3f) with prevailing wind velocity, WI is often intermittent (Figure 3a) suggesting the local effects of wind gusts buffeting against the cliff face and top. WI sometimes coincides with increased signal power in MS and HT frequencies (Figure 3c and 3f) indicating that the winds generating WI are also concomitantly generating local waves.

[25] During the two storm periods considered (Figure 3c and 3f), increases in wave height and onshore wind velocity increase signal power in all three frequency bands. Onshore winds generate storm surges that increase at-coast water elevations, forcing the surf zone inland beyond the still water line. This also produces a HT signal during neap tide storms (Figure 3c). The increase in power of HT during storms persists beyond the normal tidal inundation defined by the still water elevation. By implication, in addition to periods of elevated mean water level and greater incident wave energy, wave breaking and turbulent water within surf across the foreshore may therefore generate high power signals in HT (Figures 3c and 3f).

[26] Examining signal power spectrograms over a neap to spring tidal cycle (2 weeks) highlights the short-term variability in each of the frequency bands; a response clearly dependent on the marine and wind conditions (Figure 4) which echoes observations made over single tidal cycles. The presence of higher powers in the MS and HT bands demonstrate the presence of larger waves and the impact of onshore waves on the cliff or foreshore during surges or when spring high tide water levels are at the cliff face. The occurrence of high-power MS signals without concurrent high power HT signals indicates either seismic sources (waves) at distal locations, or that during neap tides waves are unable to impact the cliff face.

[27] The 2 year time series of tides, wave height and wind velocity local to the cliff demonstrate high variability in conditions experienced by the cliff and clear seasonality (more clearly defined in the smoothed data), with more energetic wave and wind conditions during winter months (Figure 5a, 5b, and 5c). Wind and atmospheric pressure changes in the North Sea are governed by the pressure gradient of the North Atlantic Oscillation (NAO) [OSPAR, 2000]. The cyclic nature of wind velocity (Figure 5c), particularly during winter months, is due to the stronger and more variable winter NAO [*Wakelin et al*., 2003]. Within the 2 year spectrogram a seasonal pattern can be seen across the range of microseisms (MS) presented (1–10 s) (Figure 5d). This reflects the seasonality of wave heights (Figure 5b) with highest MS powers occurring during winter months when the bandwidth of responsive frequencies also increases. Longer winter MS wave periods in the spectrogram (Figure 5d) may represent swell waves arriving from storm locations some distance from the coast, generated by high wind velocities, which may have travelled and developed over larger fetch distances. Within the 2 year spectrogram the consistent nature of the anthropogenic (AN) frequency band is clear and with no evidence of seasonal variation, supporting the conclusion that these signals are man-made (Figure 5d). The high-frequency HT and WI bands remain difficult to characterise at this resolution (Figure 5d). Typically increased power appears to occur concurrently with higher power in the MS band. Higher power often occurs as a result of clusters of events, suggesting the occurrence of storms or stormy periods.

[28] The 2 year time series of the spectral energy of individual periods in the WI (0.022 s) (Figure 6a) and MS (1, 2, and 5 s) (Figure 6c, 6d, and 6e) frequency bands depict seasonality, with higher energy being transferred via the wind (WI) and microseism (MS) mechanisms during winter months, when higher wind velocities and wave heights occur (Figure 5b and 5c). HT (0.104 s) (Figure 6b) does not display seasonality which likely represents the importance of spring tides in determining the occurrence of this signal which occur all year round (Figure 5a), or the relatively constant AN source.

4.1.3. Spatial Variability – Cross-Shore Signal Decay

[29] Figure 7 considers inland energy attenuation relative to the signal recorded at S1 at the cliff-top edge. During high spring tides (Figure 7a) when the sea is at the cliff face the individual periods that have been selected here to represent WI (0.022 s) and HT (0.104 s), both decay significantly inland from the cliff edge. This landward decay demonstrates that in HT the apparently marine dominated signal saturates AN. The increase in WI energy ratio at S4 is attributed to local wind noise around that particular instrument, due to the proximity of a fence. The MS periods (1 s, 2 s, and 5 s) show an attenuation in signal energy with distance from the cliff edge, an effect more pronounced in the shorter period signals. Seismic wave attenuation varies with frequency, with higher frequency waves attenuating quicker than longer periods [*Lowrie*, 1997]. The observed cross-shore decay patterns may therefore represent variable attenuation for different frequencies consistent with previous studies [*Young et al*., 2012]. If cross-shore decay is representative of source locality then the stronger attenuation of WI and HT compared to MS indicates WI and HT are generated more locally to the cliff face, in accordance with the cliff face mechanisms we associate with each. All three MS periods may represent local

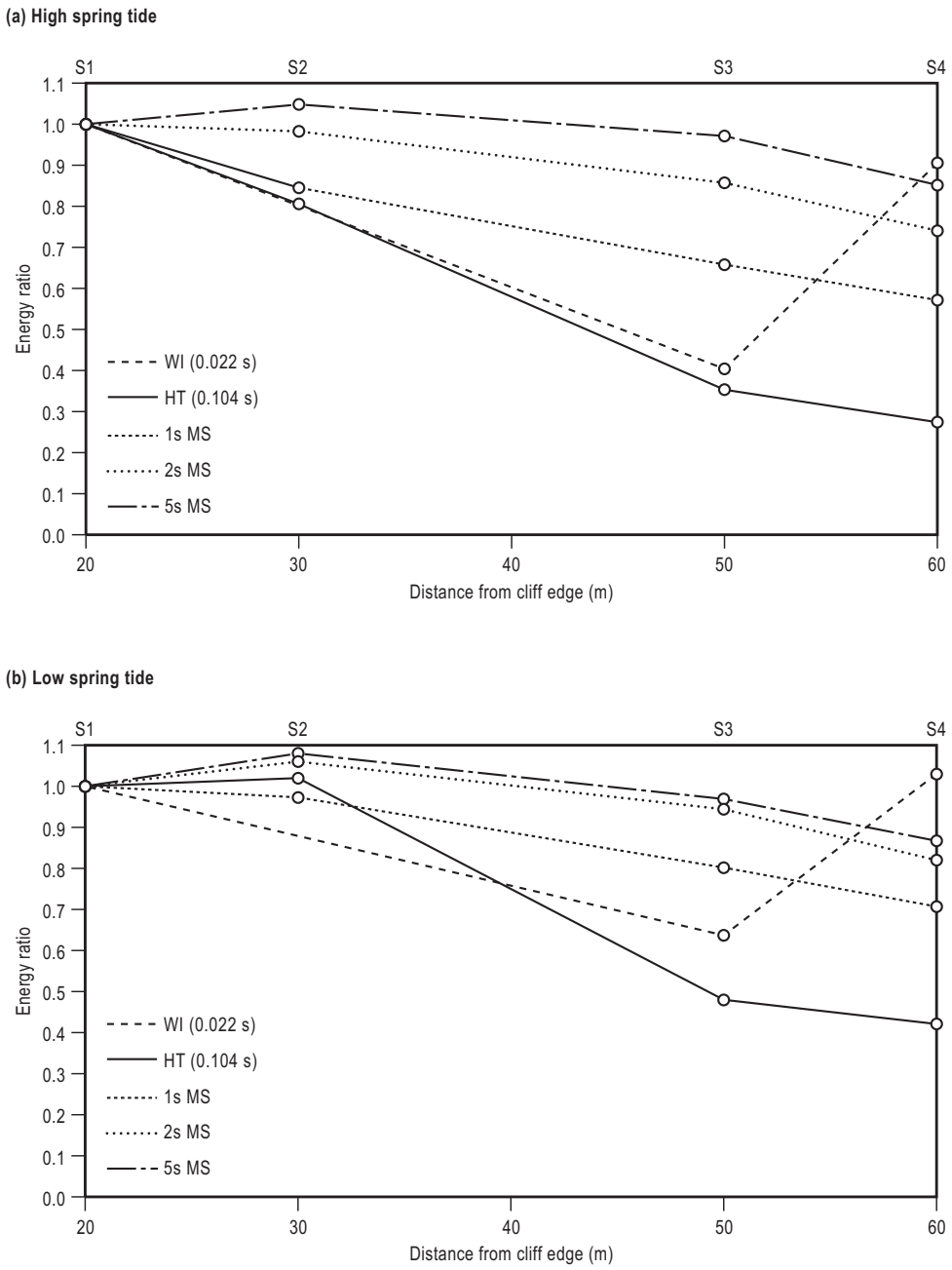

Figure 7. Energy ratio between each seismometer (S2–S4) and the cliff-edge seismometer (S1) during: (a) High spring tides; (b) Low spring tides. Ground motion periods selected to represent the three ground motion frequency bands are: WI (0.022 s); HT (0.104 s); 1 s MS; 2 s MS and 5 s MS.

single frequency microseisms or double frequency microseisms that could be generated over a larger area, but the weaker decay of the 5 s period may suggest a greater proportion of this signal is generated by more distal double frequency microseisms. There may also be an overlap with HT at the lower MS periods.

[30] During low spring tides (Figure 7b) when the still water line is approximately 200 m seawards of the cliff toe, all signals have a similar decay pattern as during high tides (Figure 7a), although the decay with distance is less. This is likely due to the greater distance to the water's edge and therefore marine sources. The low tide decay of WI suggests that wind transfers energy via the sea surface in addition to directly to the cliff face, or may reflect the overlap with the HT signal.

4.2. Energy and Water Level

[31] We consider how energy transfer varies with water elevation and the combined effects of tide, wave and set-up heights by aggregating modelled and monitored water elevation and duration over the monitoring period (Figure 8a). Using this approach we observe a net elevation increase in the combined inundation signature as compared to still water tidal inundation duration alone (Figure 8a).

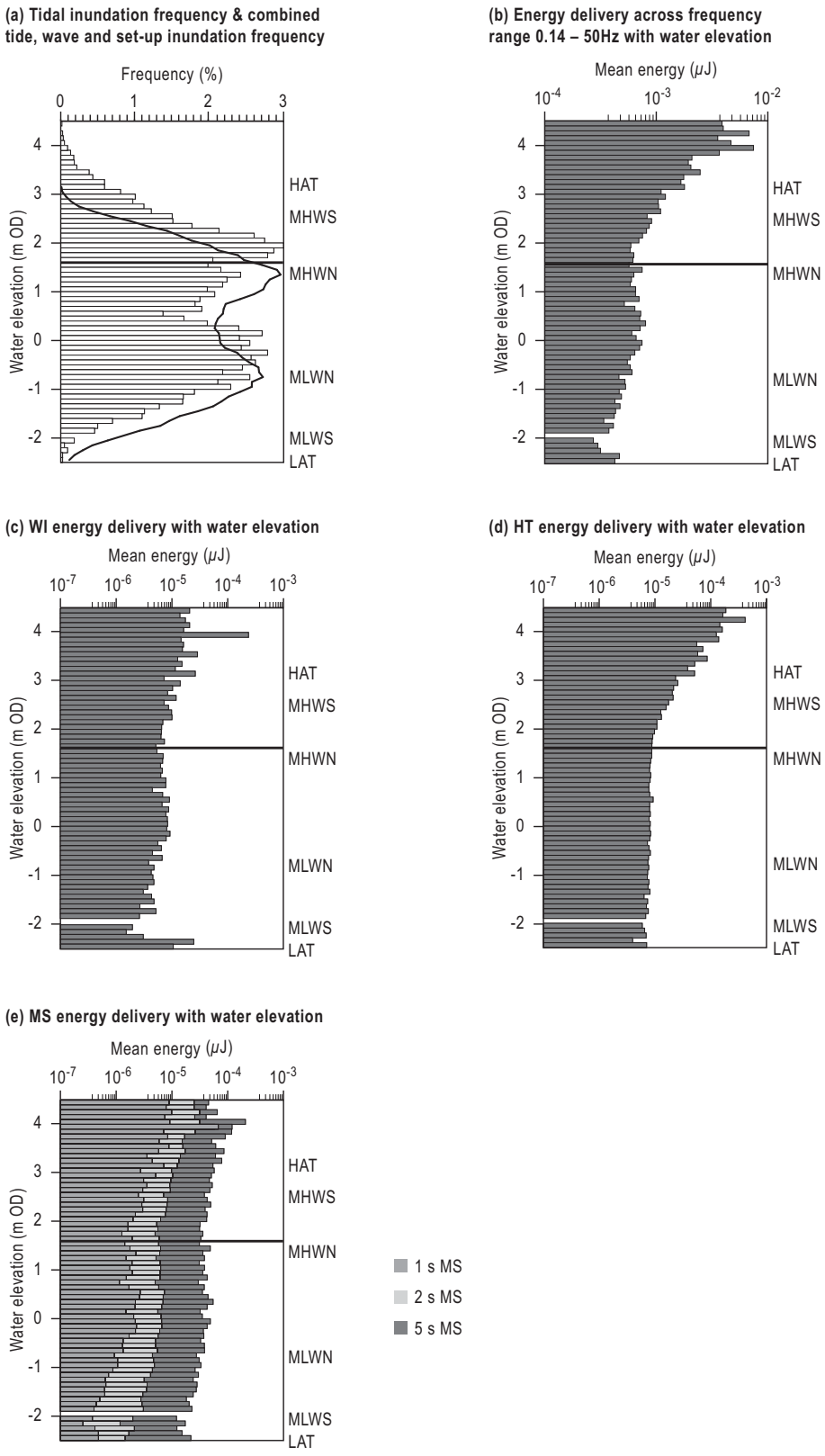

Figure 8. (a) Modelled tidal inundation frequency for Boulby (line) and combined tide & surge (monitored), wave and set-up elevations (modelled) at Boulby (bars). Mean hourly energy transfer with water elevation for: (b) the frequency range 0.14–50 Hz (0.02–7 s); (c) wind, WI (0.022 s); (d) high tide wave impacts, HT (0.104 s); e) microseisms, MS (1 s, 2 s, and 5 s). Water elevations are divided into 0.1 m bins, and hourly mean energy (b – e) and inundation frequency (a) per 0.1 m bin have been calculated over the 2 year monitoring period. The black horizontal line marks the cliff toe elevation at 1.6 m OD.

[32] We examine the mean hourly ground motion energy over the 2 year monitoring period across the signal period range 0.02–7 s (0.14–50 Hz) (Figure 8b) and for the representative periods from each frequency band (Figures 8c–8e), again aggregated by modelled water elevation combining tide, wave and set-up heights. Several key observations of the vertical signature of energy transfer follow:

[33] 1. The pattern of mean energy delivery for each 0.1 m bin of water elevation across 0.02–7 s (8b) shows considerable departure to the tide-only and combined water level inundation duration models (8a). A net increase in energy delivery with respect to increased sea water elevation is clear, with a subtle increase in signal energy at water elevations between Lowest Astronomical Tide (LAT) and the cliff toe elevation. A pronounced increase also occurs up cliff (8b). Peak mean energy delivery and maximum variability in mean energy between contiguous elevation bands coincides with maximum water levels (Figure 8b). For the combined spectrum of processes considered here, peak energy delivery to the cliff is therefore not determined by tidal inundation frequency, but by storm and swell wave magnitude.

[34] 2. As the WI band is largely determined by wind velocity and not water elevation, the increase in WI (0.022 s) energy transfer at higher water elevations (Figure 8c) is believed to reflect the high wind velocities at the cliff during storms (when water elevations are raised), with possible signal contamination from additional wind driven waves during storms. Whilst there is some overlap between HT and WI, the periods selected to represent these bands are selected from the parts of each band least affected by the other. A similar peak in the seismic signal that corresponds with extreme low water levels (< -2.2 m OD) may reflect winds acting upon and exciting a fully exposed foreshore.

[35] 3. In HT (Figure 8d) energy transfer increases with water elevation once the water level reaches the cliff toe. During water elevations below the cliff toe elevation, HT (0.104 s) energy is non-zero but constant, showing no relationship with falling or rising water elevation. The constant background noise is believed to most probably result from anthropogenic sources. Modelling tides, waves and set-up (Figure 8a) demonstrates that water elevations significantly exceed those reached by high tides alone, and importantly HT demonstrates that maximum signal energy occurs during the highest water elevations. HT is the frequency band, at least logically, that is most directly related to those processes that are reliant upon the presence of sea water at the cliff toe, yet shows the greatest departure in form of all frequency bands from the tidal inundation distribution (8a).

[36] 4. MS at specific frequencies (1 s, 2 s, and 5 s) (Figure 8e) show that signal energy increases as the tide level rises up the cliff face, with peak signal energy occurring at the highest water levels. This pattern is more defined for shorter period signals (1 s & 2 s). The cross-shore decay plots (Figure 7) imply that some portion of these three MS signals are generated locally across the foreshore, which may either be single or double frequency microseisms. The peak in this signal represents increasing energy transfer from both mechanisms acting upon the foreshore during increasingly stormy conditions as waves producing the microseisms are larger and more energetic. In addition during high water levels this peak may represent the effects of storm conditions more widely including larger swell waves transmitting greater signal energy as double frequency microseisms across a wide area, particularly in the longer 5 s period, a period which shows the least variability with water level (Figure 8e).

[37] By plotting mean hourly energy rather than the sum of hourly energy for each water level during the two-year period we can examine the magnitude of energy transferred to the cliff during typical events that occur at each water level. We anticipate that this is more important in determining erosion, i.e., low frequency high energy transfer events (e.g., as occurs when water levels are higher up the cliff face), are more important in determining erosive work than low energy transfer that occurs more frequently (e.g., as in the mid-tide zone).

5. Discussion

5.1. Marine and Wind Generated Cliff Ground Motions and Potential Erosion Implications

5.1.1. Microseisms (MS)

[38] Single frequency microseisms are generated in shallow water via pressure fluctuations beneath waves in water depths of half the wave wavelength [*Hasselmann*, 1963; *Hedlin and Orcutt*, 1989], generated predominantly by waves transiting across the intertidal foreshore. In global noise models single frequency microseisms are typically observed in the range 10–16 s [*Peterson*, 1993; *McNamara and Buland*, 2004], as discussed in cliff microseismic studies elsewhere [e.g., *Adams et al*., 2005; *Young et al*., 2011, 2012]. We have observed shorter period signals at this site, the cross-shore decay of which suggests these signals represent shorter period wave processes, and potentially single frequency microseisms, in the shallow coastal water. Short period ocean waves are easily generated: 2 s waves have been observed to form in 2.5 h under wind of only 5 ms^{-1} [*Webb*, 1998], which is highly feasible within the North Sea fetch. The shallow coastal waters, wide foreshore and large tidal range of the site provide an extensive area over which shorter period single frequency microseisms can be generated.

[39] Assuming cross-shore signal decay represents relative source proximity rather than solely frequency-controlled attenuation, the enhanced decay of the 1 s MS signal may indicate it is not generated over such an extensive area as the 2 s and 5 s MS signals, which complies with the shallower water depths required for shorter wavelength, short period waves to generate single frequency microseisms [*Haubrich et al*., 1963; *Hedlin and Orcutt*, 1989]. Seismic signals of 1 s period are common at ocean bottom seismic stations, as the sea surface responds quickly to local winds and these short period waves attenuate rapidly [*Webb*, 1998]. In addition to wind surface waves, the 1 s intertidal signal may also represent wave breaking within shallow coastal waters, which has been observed to generate ocean bottom seismic signals around the 1 s period [*McCreery et al*., 1993]. The wave model showed the majority of waves break in the 500 m before the cliff, across the wide foreshore and shallow waters beyond, providing a wide area over which this signal may be generated.

[40] The generation of short-period waves by gentle winds mean that superposition of these waves to form short-period (< 5 s) double frequency microseisms can occur as wind directions shift and waves travelling from opposing directions interfere, as observed elsewhere [e.g., *Kibblewhite and Ewans*, 1985]. Alternatively, waves reflected by the coast may superimpose with incoming waves of the same period. Although such waves occur frequently, short-period ocean waves are of small magnitude, and therefore their net amplitudes will only generate relatively low microseism power compared to larger, longer period waves generated further afield. The cross-shore decay of the MS signal may also represent shorter period double frequency microseisms generated by these processes across the intertidal foreshore, as well as in deeper local waters.

[41] It is not possible to separate the single from double frequency microseisms in the 1–5 s ground motion signal, however the low cross-shore attenuation of 5 s MS suggests near-coast single frequency microseisms. Approximately 20% of waves recorded at the wave buoy have 5 s periods. This observation differs from *Young et al*. [2012] who did not observe cross-shore decay in the double frequency range suggesting that at their site this signal represented distal microseismic sources. Differences in MS signal decay between sites may be explained by varying local seabed and foreshore topography and geology, and water depths, where the wide, gentle gradient foreshore and coastal seabed of this site and the relatively shallow waters of the North Sea compared to the Pacific are highly suitable for single frequency microseism generation [*Hedlin and Orcutt*, 1989].

[42] Cliff top microseismic studies on the US Pacific coast have examined single frequency microseisms at longer periods (10–20s) [*Adams et al*., 2005; *Young et al*., 2011]. Because of the limited fetch of the North Sea compared to the Pacific, it is anticipated that longer period single frequency microseisms are not as frequently generated in the North Sea. Only 8% of the monitored maximum wave periods recorded at the wave buoy are 10 s, and only 1% are 15 s or longer.

[43] The higher signal powers in MS during low wave conditions monitored at the buoy (Figures 2, 3, and 4) demonstrate that some of the microseisms detected at the seismometer are not generated at this coast. A number of previous studies have detected primary microseisms generated at other coastal locations, whilst not at the seismometer location [e.g., *Cessaro*, 1994; *Friedrich et al*., 1998]. This suggests that the single frequency microseisms observed here may be generated on other coasts within the relatively confined North Sea basin. The p-wave component of double frequency microseisms in the range 2.86–6.25 s generated by storms in distant oceans can be detected on land-based seismometers [*Zhang et al*. 2010], and therefore some of the 5 s double frequency microseism signal may represent these wave sources $> 10^3$ km away.

5.1.2. High Tide Signal (HT)

[44] HT is generated by wave impacts against a relatively small inundated area of rock at the cliff toe, the extent and timing of which is modulated by the tide and the occurrence of sufficiently large waves (Figure 3), also observed by *Adams et al*. [2005] and *Dickson and Pentney* [2012]. Waves break at the cliff face, but the wave model results [presented in *Norman*, 2012] indicate most will break before the cliff between LAT (250 m from cliff) and MLWS (200 m from cliff) due to the long gentle gradient (< 2°) of the foreshore meaning that it is commonly turbulent surf that directly contacts the cliff. Although the foreshore is wide, the tidal range means that water depths across the foreshore are sufficient during spring tides for large waves to reach the cliff toe, whereby sufficient energy is retained within the wave field to generate high-frequency shaking of the cliff on impact. The resulting horizontal loading, vertical shearing via wave run- both up and down the cliff face, and vertical loading of the cliff face and foreshore due to vertical forces as the wave crest collapses [*Wolters et al*., 2005; *Hansom et al*., 2008; *Müller et al*., 2008], are all important in removing cliff material via hydraulic action and abrasion. Due to the high energy transfer rates during periods of high tide wave impacts (Figures 2, 3, and 4), we propose that the erosive processes driven by impact pressures such as quarrying and attrition will also occur most efficiently during these periods.

[45] The high signal power in the HT frequency band (Figures 2, 3, and 4), and the tidal cycle that defines when those processes seen in HT are acting on the cliff rock face most effectively, implies that despite the comparatively small source area and limited time window, the efficiency of this mechanism of energy transfer is higher, and hence is potentially far more geomorphologically effective, than those processes represented by MS frequencies.

[46] Thresholds of combined tide and wave heights are key for the generation of the HT signal at this site, as also observed by *Adams et al*. [2005] and *Dickson and Pentney* [2012]. Whilst other studies have observed tidal controls on this signal [e.g., *Young et al*., 2011, 2012], the tidal control has not been so pronounced, possibly due to more narrow, steeper foreshores and more limited tidal ranges. At this site, high spring tides or storm surges are necessary in order to generate HT signals, as at these tide heights the waterline moves up the cliff face and water depths across the foreshore are sufficient for wave energy to remain in the wave field until reaching the cliff. In addition the shallow gradient foreshore at this site means that during storms when greater wave energy is available HT has also been observed to be generated by the same mechanisms on the foreshore near the cliff toe, which has not been observed at the other sites of other studies [e.g., *Adams et al*., 2005; *Young et al*., 2011, 2012; *Dickson and Pentney*, 2012]. Foreshore elevation relative to the tidal range is key in determining when and hence where peak HT energy transfer occurs: *Dickson and Pentney* [2012] observed peak wave impact energy transfer to occur during low tides as waves impacted against the seaward edge of a raised horizontal platform, and during high tides shallow water depths over the foreshore dissipated wave energy before it reached the cliff toe, thus producing no equivalent high tide impact signal to that observed here.

5.1.3. Wind (WI)

[47] The WI signal is most energetic during high velocity onshore winds (Figures 2, 3, and 4), which we suggest is associated with the transfer of energy via wind loading of the cliff, and large-scale turbulence generated by the abrupt cliff geometry [*McNamara and Buland*, 2004; *Bormann*,

2009]. At our site this signal can be generated both upon the cliff top ground surface, and at the cliff face. Qualitatively there is evidence of high velocity onshore winds travelling up and over the cliff top. As winds travel across the cliff face, shearing forces occur that may dislodge loose material. The presence of the seismometer boxes which house batteries and cabling, and the solar panels on the surface above the seismometers may increase ground friction and generate additional localised turbulence. Further, and in particular at the most landward instrument, fencing may also have a similar effect particularly where well coupled to the ground [*McNamara and Buland*, 2004] (Figure 7). The highest power WI signal is produced during periods of onshore winds, which implies that in addition to turbulence at the cliff face, wind loading also transfers energy to the cliff via buffeting. This characteristic of coastal cliff motion has not previously been quantified however the signal characteristics match those observed by studies of wind seismic noise in other settings [e.g., *Withers et al*., 1996; *Young et al*., 1996; *McNamara and Buland*, 2004].

[48] Generation of WI during periods of offshore winds and the cross-shore decay of WI during low tides, suggest that wind also generates this signal via interaction with the sea surface [e.g., *Webb*, 1998]. Similar high frequency signals recorded on ocean bottom seismometers have also been found to correlate well with local wind velocities, thought to represent acoustic signals generated by white-capped waves on the sea surface [*McCreery et al*., 1993]. These results are important as they identify that energy is not only delivered to the cliff from marine sources.

5.2. Energy Transfer and Water Elevation

[49] The microseismic cliff ground motion reported identifies that energy transfer is significantly more complex than a summation of tidal inundation duration at the cliff toe, an approach which often forms the basis of coastal cliff erosion models [e.g., *Trenhaile*, 2000; *Walkden and Hall*, 2005; *Walkden and Dickson*, 2008; *Trenhaile*, 2009, 2011; *Ashton et al*., 2011]. Typically one of two approaches to equate marine energy transfer to erosion of the cliff toe is adopted: i) the vertical extent and frequency of occurrence of the mean sea surface level (inundation duration) using predicted tide height distributions [e.g., *Trenhaile*, 2000]; and, ii) the vertical extent of monitored total water levels, which sum tide and meteorological effects including surges, waves, and wave run-up [e.g., *Benumof et al*., 2000; *Ruggiero et al*., 2001]. Our results demonstrate that the combined height of tides and waves (incorporating surge and set-up effects) determined by foreshore/beach characteristics, determine when marine energy transfer to the cliff face occurs (Figures 3 and 8). The inundation duration model derived from combined effects of waves, set-up, surges and tides retains the bi-modal distribution typical of semi-diurnal tidal inundation duration models (Figure 8a) [e.g., *Carr and Graff*, 1982; *Trenhaile*, 2009]. Figure 8 shows that even accounting for waves and surges, the inundation duration does not define when peak energy transfer occurs. Instead peak energy transfer across the analysed spectrum (0.14–50 Hz) occurs when water levels at the cliff face are deepest (Figure 8b); commonly, when the largest storms raise coastal water levels and enable greater wave, set-up and run-up heights directly at the cliff face.

[50] Tidal inundation duration models have been adopted within numerical models of cliff erosion, to predict where wave erosive processes are concentrated and how cliff erosion relates to absolute sea level [e.g., *Walkden and Hall*, 2005; *Dickson et al*., 2007; *Walkden and Dickson*, 2008; *Ashton et al*., 2011]. Models based upon inundation duration suggest energy delivery and hence erosion is likely to be focussed around high and low tide levels where the tide level spends the greatest proportion of time [*Carr and Graff*, 1982]. Within these models erosion is understood to be concentrated at an elevation just above peak tidal inundation duration, resulting from the elevated additional influence of wave impacts, wherein the combination of air and water enable increased hydraulic impact pressures and the mechanical attrition and abrasion, resulting in removal of material from the cliff [*Trenhaile*, 2000]. The HT frequency band appears to most closely represent these processes at the cliff face. Previously the distribution of energy delivery to the cliff resulting from tidal inundation has not been quantified to consider how well these models represent the erosive efficacy of wave energy at the cliff toe. Our results indicate that mean energy transfer, which we assume to be a proxy for erosion potential, increases in the HT signal with water depth above the cliff toe, notably during stormy conditions. Our results suggest that if energy transfer via direct wave impacts is a proxy for erosion, then it is the time-distribution of peak energy transfer (8d) that is likely more important in determining the vertical profile of erosion as opposed to the frequency of occurrence of low energy transfer defined by tidal inundation alone.

[51] Energy transfer aggregated by water level reflects the energy budget of the coast more widely, from across the foreshore and beyond. The water level and energy transfer graphs therefore do not solely represent energy transfer directly at these water levels at the cliff but the general energy state across the coastal zone, and also anthropogenic noise and non-local sources. For example, the energy transfer from single and double frequency microseisms.

5.3. Using Cliff-Top Motions as Proxies for Environmental Processes on Coastal Cliffs

[52] The 2 year dataset of cliff motions has enabled examination of the characteristics and temporal variability of three frequency bands of ground motion, and how each correspond to changing environmental conditions both at the coast and more distally. The length of the dataset enables exploration of the full range of seasonal conditions the cliff experiences and the resulting ground motion response. The dataset demonstrates the importance of combined tide, wave and weather conditions in determining the seismic ground motion, and that considering these variables individually does not provide an accurate depiction of conditions affecting the cliff. Because of the complex interactions between the various marine and non-marine variables, obtaining a measure of the conditions the cliff actually experiences is complex and therefore testing the environmental conditions that erode cliffs is also difficult. A key challenge remains in linking these data, and similar datasets elsewhere to the actual processes of erosion. Whilst using cliff-top microseisms as proxies for the marine and non-marine/environmental processes that

transfer energy to cliffs may help overcome previous limitations in monitoring, linking this directly to erosion and cliff failure remains problematic. The monitored cliff-top ground motion demonstrates the range of sources which transfer energy to the cliff and puts these into relative terms.

[53] Cliff-top ground motions have now been observed in a number of rock-cliff settings of varying geology, coastal morphology, wave and weather climates [e.g., *Adams et al*., 2002; *Adams et al*., 2005; *Lim et al*., 2011; *Young et al*., 2011, 2012; *Dickson and Pentney*, 2012]. The differences in signal characteristics between these studies demonstrate that cliff motions provide accurate representation of local environmental processes acting on the cliffs, but that they are heavily conditioned by local and regional physiographic characteristics. We argue that cliff-top motions therefore have the potential to be important in quantitatively testing environmental controls of cliff erosion, and in providing a transferrable measure that may directly relate to erosion across sites, which may enable process comparison.

[54] There are challenges in using cliff-top motions as proxies of both marine and non-marine processes, related to identifying the exact source location and character, period overlap with local and regional noise sources, and potentially high levels of tilt contamination [*McNamara and Buland*, 2004; *Bormann*, 2009] particularly in longer period ground motions that cause greater displacements [*Young et al*., 2011]. Using an array of seismometers distributed along the coastline, and inland from the coastline can assist in isolating source locations [e.g., *Cessaro*, 1994; *Friedrich et al*., 1998], which can also help attributing source and distinguishing environmental from anthropogenic signals.

6. Conclusions

[55] Our 2 year dataset described cliff-top ground motions over the range of environmental conditions experienced on a storm-dominated rocky coastal cliff. We have demonstrated that three characteristic frequency bands of motion within the frequency range 0.14–50 Hz (0.02–7 s) are coincident with temporal variations in forcing from a number of wind and wave processes from which we conclude transfer energy to the cliff rock mass. Our data suggest that these processes operate over a range of locations both local and distal to the cliff; directly at the cliff face, across the intertidal foreshore and at more distal locations offshore within the North Sea basin and beyond, and each show a strong temporal relationship with prevailing wind, tide and wave conditions. Combinations of tide, wave and wind conditions are important for energy transfer and cliff-top ground motions provide an indicator of when these combined conditions and energy transfer to the cliff occur, overcoming the difficulties of monitoring these variables directly and locally to the coast. Our data also demonstrate that foreshore and cliff-toe elevation relative to the tidal range are key in determining local water depths relative to the cliff and therefore where energy transfer occurs.

[56] Peak energy transfer to the cliff face occurs during the largest storms where water levels significantly exceed those of tidal inundation rather than at locations most frequently inundated by the tides. It is therefore these conditions that are likely to be most effective in eroding hard rock coasts, rather than periods which accrue energy transfer associated with still or calm waters, and hence tidally modulated inundation may not relate well to hard rock cliff erosion.

[57] Promisingly cliff-top motions can be used as proxies for the processes that transfer energy to the cliff and coast, and we anticipate that such datasets will prove useful tools in exploring environmental controls of erosion. There are some difficulties in using ground motions as proxies for energy transfer processes, caused by the overlap of signals generated by different processes, and local and non-local noise. Future work will focus upon relating environmental processes represented by ground motion to high resolution erosion monitoring datasets.

[58] **Acknowledgments.** The authors wish to thank the Natural Environment Research Council Geophysical Equipment Facility for the loan of the seismic equipment (loan number 879), SEIS-UK for their technical support and advice throughout the project and Cleveland Potash Ltd who fund this research. Wave buoy data was provided by the Centre for Environment, Fisheries and Aquaculture Science, tide gauge data was provided by the British Oceanographic Data Centre and weather data from the British Atmospheric Data Centre.

References

Adams, P. N., R. S. Anderson, and J. Revenaugh (2002), Microseismic measurement of wave-energy delivery to a rocky coast, *Geology*, *30*(10), 895–898, doi:10.1130/0091-7613(2002)030<0895:MMOWED>2.0.CO;2.

Adams, P. N., C. D. Storlazzi, and R. S. Anderson (2005), Nearshore wave-induced cyclical flexing of sea cliffs, *J. Geophys. Res.*, *110*, F02002, doi:10.1029/2004jf000217.

Agar, R. (1960), Post-glacial erosion of the North Yorkshire coast from the Tees estuary to Ravenscar, *Proc. Yorkshire Geol. Soc.*, *32*(4), 409–428.

Anderson, R. S., A. L. Densmore, and M. A. Ellis (1999), The generation and degradation of marine terraces, *Basin Res.*, *11*(1), 7–19.

Ashton, A. D., M. J. A. Walkden, and M. E. Dickson (2011), Equilibrium responses of cliffed coasts to changes in the rate of sea level rise, *Mar. Geol.*, *284*(1–4), 217–229, doi:10.1016/j.margeo.2011.01.007.

Barlow, J., M. Lim, N. Rosser, D. Petley, M. Brain, M. Geer, and E. Norman (2012), Modeling cliff erosion using negative power law scaling of rockfalls, *Geomorphology*, *139–140*, 416–424, doi:10.1016/j.geomorph.2011.11.006.

Battjes, J. A., and M. J. F. Stive (1985), Calibration and verification of a dissipation model for random breaking waves, *J. Geophys. Res.*, *90*(NC5), 9159–9167, doi:10.1029/JC090iC05p09159.

Benumof, B. T., C. D. Storlazzi, R. J. Seymour, and G. B. Griggs (2000), The relationship between incident wave energy and seacliff erosion rates: San Diego County, California, *J. Coastal Res.*, *16*(4), 1162–1178.

Bormann, P. (2009), Seismic signals and noise, in *New Manual of Seismological Observatory Practise (NMSOP-1)*, edited by P. Bormann, IASPEI, GFZ Ger. Res. Cent. for Geosci., Potsdam, Germany, 1–62, doi:10.2312/GFZ.NMSOP_r1_ch4.

Brain, M. J., N. J. Rosser, E. C. Norman, and D. N. Petley (2013), Are microseismic ground displacements a significant geomorphic agent? *Geomorphology*, doi:10.1016/j.geomorph.2013.11.002, in press.

Bray, M. J., and J. M. Hooke (1997), Prediction of soft-cliff retreat with accelerating sea-level rise, *J. Coastal Res.*, *13*(2), 453–467.

Bromirski, P. D., and F. K. Duennebier (2002), The near-coastal microseism spectrum: Spatial and temporal wave climate relationships, *J. Geophys. Res.*, *107*(B8), 2166, doi:10.1029/2001JB000265.

Bungum, H., S. Mykkeltveit, and T. Kvaerna (1985), Seismic noise in Fennoscandia, with emphasis on high-frequencies, *Bull. Seismol. Soc. Am.*, *75*, 1489–1513.

Carr, A. P., and J. Graff (1982), The tidal immersion factor and short platform development—discussion, *Trans. Inst. Br. Geogr.*, *7*(2), 240–245, doi:10.2307/622227.

Cessaro, R. K. (1994) Sources of primary and secondary microseisms, *Bull. Seismol. Soc. Am.*, *84*, 142–148.

Collins, B. D., and N. Sitar (2008), Processes of coastal bluff erosion in weakly lithified sands, Pacifica, California, USA, *Geomorphology*, *97*(3–4), 483–501, doi:10.1016/j.geomorph.2007.09.004.

Dewez, T., D. Gebrayel, D. Lhomme, and Y. Robin (2009), Quantifying morphological changes of sandy coasts by photogrammetry and cliff coasts by lasergrammetry, *Houille Blanche-Rev. Int.*, (1), 32–37, doi: 10.1051/lhb:2009002.

Dickson, M. E., M. J. A. Walkden, and J. W. Hall (2007), Systemic impacts of climate change on an eroding coastal region over the twenty-first century, *Clim. Change*, *84*(2), 141–166, doi:10.1007/s10584-006-9200-9.

Dickson, M. E., and R. Pentney (2012), Micro-seismic measurements of cliff motion under wave impact and implications for the development of near-horizontal shore platforms, *Geomorphology*, *151*, 27–38, doi: 10.1016/j.geomorph.2012.01.006.

Friedrich, A., F. Kruger, and K. Klinge (1998), Ocean-generated microseismic noise located with the Grafenberg array, *J. Seismol.*, *2*, 47–64, doi: 10.1023/A:1009788904007.

Given, H. K. (1990), Variations in broad-band seismic noise at IRIS/IDA stations in the USSR with implications for event detection, *Bull. Seismol. Soc. Am.*, *80*(6), 2072–2088.

Gurrola, H., J. B. Minster, H. Given, F. Vernon, J. Berger, and R. Aster (1990), Analysis of high frequency seismic noise in the western United-States and eastern Kazakhstan, *Bull. Seismol. Soc. Am.*, *80*, 951–970.

Hansom, J. D., N. D. P. Barltrop, and A. M. Hall (2008), Modelling the processes of cliff-top erosion and deposition under extreme storm waves, *Mar. Geol.*, *253*(1–2), 36–50, doi:10.1016/j.margeo.2008.02.015.

Hapke, C. J., and K. R. Green (2006), Coastal landslide material loss rates associated with severe climatic events, *Geology*, *34*(12), 1077–1080, doi:10.1130/G22900A.1.

Hasselmann, K. (1963) A statistical analysis of the generation of microseisms, *Rev. Geophys.*, *1*, 177–210, doi:10.1029/RG001i002p00177.

Haubrich, R. A., W. H. Munk, and F. E. Snodgrass (1963), Comparative spectra of microseisms and swell, *Bull. Seismol. Soc. Am.*, *53*, 27–37.

Hedlin, M. A. H., and J. A. Orcutt (1989), A comparative study of island, seafloor, and subseafloor ambient noise-levels, *Bull. Seismol. Soc. Am.*, *79*(1), 172–179.

Kibblewhite, A. C., and K. C. Ewans (1985) Wave-wave interactions, microseisms, and infrasonic ambient noise in the ocean, *J. Acoust. Soc. Am.*, *78*, 981–994, doi:10.1121/1.392931.

Lim, M., J. Mills, and N. Rosser (2009), Laser scanning surveying of linear features: Considerations and applications, in *Laser Scanning for the Environmental Sciences*, edited by G. Heritage and A. Large, pp. 245–261, Wiley-Blackwell, Chichester, U. K.

Lim, M., N. J. Rosser, R. J. Allison, and D. N. Petley (2010), Erosional processes in the hard rock coastal cliffs at Staithes, North Yorkshire, *Geomorphology*, *114*(1–2), 12–21, doi:10.1016/j.geomorph.2009.02.011.

Lim, M., N. J. Rosser, D. N. Petley, and M. Keen (2011), Quantifying the controls and influence of tide and wave impacts on coastal rock cliff erosion, *J. Coastal Res.*, *27*(1), 46–56, doi:10.2112/jcoastres-d-09-00061.1.

Longuet-Higgins, M. S. (1950), A theory of the origin of microseisms, *Philos. Trans. R. Soc. London A*, *243*, 1–35.

Lowrie, W. (1997), *Fundamentals of Geophysics*, Cambridge Univ. Press, Cambridge, N. Y.

McCreery, C. S., F. K. Duennebier, and G. H. Sutton (1993) Correlation of deep ocean noise (0.4–30 Hz) with wind, and the Holu spectrum—a worldwide constant, *J. Acoust. Soc. Am.*, *93*, 2639–2648, doi:10.1121/1.405838.

McNamara, D. E., and R. P. Buland (2004), Ambient noise levels in the continental United States, *Bull. Seismol. Soc. Am.*, *94*(4), 1517–1527, doi:10.1785/012003001.

Müller, G., W. Allsop, T. Bruce, A. Kortenhaus, A. Pearce, and J. Sutherland (2008), The occurrence and effects of wave impacts, *Proceedings of the Institution of Civil Engineers*, *160*(MA4), 167–173, doi: 10.1680/maen.2007.160.4.167.

Norman, E. C. (2012) Microseismic monitoring of the controls on coastal rock cliff erosion, PhD Thesis, Durham Univ., Durham, U. K. Durham University open access eTheses repository. [Available at http://etheses.dur.ac.uk/3586/.]

OSPAR (2000) *Quality Status Report 2000*, OSPAR, London.

Peterson, J. (1993), Observations and modeling of seismic background noise, in U.S. Geological Survey, Tech. Rep. 93–322.

Quinn, J. D., N. J. Rosser, W. Murphy, and J. A. Lawrence (2010), Identifying the behavioural characteristics of clay cliffs using intensive monitoring and geotechnical numerical modelling, *Geomorphology*, *120*(3–4), 107–122, doi:10.1016/j.geomorph.2010.03.004.

Rawson, P. F., and J. K. Wright (1992), *The Yorkshire Coast*, Geologists' Association Guide no 34, Geol. Assoc., London.

Rosser, N. J., D. N. Petley, M. Lim, S. A. Dunning, and R. J. Allison (2005), Terrestrial laser scanning for monitoring the process of hard rock coastal cliff erosion, *Q. J. Eng. Geol.*, *38*, 363–375, doi:10.1144/1470-9236/05-008.

Rosser, N., M. Lim, D. Petley, S. Dunning, and R. Allison (2007), Patterns of precursory rockfall prior to slope failure, *J. Geophys. Res.*, *112*, F04014, doi:10.1029/2006jf000642.

Rosser, N. J., M. J. Brain, D. N. Petley, M. Lim, and E. C. Norman (2013), Coastline retreat via progressive failure of rocky coastal cliffs, *Geology*, doi:10.1130/G34371.1.

Ruggiero, P., P. D. Komar, W. G. McDougal, J. J. Marra, and R. A. Beach (2001), Wave runup, extreme water levels and the erosion of properties backing beaches, *J. Coastal Res.*, *17*(2), 407–419.

Sallenger, A. H., W. Krabill, J. Brock, R. Swift, S. Manizade, and H. Stockdon (2002), Sea-cliff erosion as a function of beach changes and extreme wave runup during the 1997–1998 El Nino, *Mar. Geol.*, *187*(3–4), 279–297, doi:10.1016/s0025-3227(02)00316-x.

Trenhaile, A. S. (1987), *The Geomorphology of Rock Coasts*, Oxford Univ. Press, Oxford, U. K.

Trenhaile, A. S. (2000), Modeling the development of wave-cut shore platforms, *Mar. Geol.*, *166*(1–4), 163–178, doi:10.1016/S0025-3227(00)00013-X.

Trenhaile, A. S. (2009), Modeling the erosion of cohesive clay coasts, *Coastal Eng.*, *56*(1), 59–72, doi:10.1016/j.coastaleng.2008.07.001.

Trenhaile, A. S. (2011), Predicting the response of hard and soft rock coasts to changes in sea level and wave height, *Clim. Change*, *109*(3–4), 599–615, doi:10.1007/s10584-011-0035-7.

Trenhaile, A. S., and M. G. J. Layzell (1981), Shore platform morphology and the tidal duration factor, *Trans. Inst. Br. Geogr.*, *6*, 82–102, doi: 10.2307/621974.

Wakelin, S. L., P. L. Woodworth, R. A. Flather, and J. A. Williams (2003), Sea-level dependence on the NAO over the NW European Continental Shelf, *Geophys. Res. Lett.*, *30*(7), 1403, doi:10.1029/2003GL017041.

Walkden, M. J. A., and J. W. Hall (2005), A predictive Mesoscale model of the erosion and profile development of soft rock shores, *Coastal Eng.*, *52*(6), 535–563, doi:10.1016/j.coastaleng.2005.02.005.

Walkden, M., and M. Dickson (2008), Equilibrium erosion of soft rock shores with a shallow or absent beach under increased sea level rise, *Mar. Geol.*, *251*(1–2), 75–84, doi:10.1016/j.margeo.2008.02.003.

Webb, S. C. (1998), Broadband seismology and noise under the ocean, *Rev. Geophys.*, *36*(1), 105–142, doi:10.1029/97rg02287.

Withers, M. M., R. C. Aster, C. J. Young, and E. P. Chael (1996), High-frequency analysis of seismic background noise as a function of wind speed and shallow depth, *Bull. Seismol. Soc. Am.*, *86*(5), 1507–1515.

Wolters, G., G. Müller, T. Bruce, and C. Obhrai (2005), Large-scale experiments on wave downfall pressures, *Proc. ICE*, *158*(MA4), 137–145.

Young, A. P., R. T. Guza, R. E. Flick, W. C. O'Reilly, and R. Gutierrez (2009), Rain, waves, and short-term evolution of composite seacliffs in southern California, *Mar. Geol.*, *267*(1–2), 1–7, doi:10.1016/j.margeo.2009.08.008.

Young, A. P., P. N. Adams, W. C. O'Reilly, R. E. Flick, and R. T. Guza (2011), Coastal cliff ground motions from local ocean swell and infragravity waves in southern California, *J. Geophys. Res.*, *116*, C09007, C09007doi:10.1029/2011jc007175.

Young, A. P., R. T. Guza, P. N. Adams, W. C. O'Reilly, and R. E. Flick (2012), Cross-shore decay of cliff top ground motions driven by local ocean swell and infragravity waves, *J. Geophys. Res.*, *117*, C06029, doi: 10.1029/2012jc007908.

Young, C. J., E. P. Chael, M. M. Withers, and R. C. Aster (1996), A comparison of the high-frequency (>1 Hz) surface and subsurface noise environment at three sites in the United States, *Bull. Seismol. Soc. Am.*, *86*(5), 1516–1528.

Zhang, J. A., P. Gerstoft, and P. D. Bromirski (2010), Pelagic and coastal sources of P-wave microseisms: Generation under tropical cyclones, *Geophys. Res. Lett.*, *37*, L15301, doi:10.1029/2010gl044288.